metals

MDPI

Article

Impact of Warm Rolling Process Parameters on Crystallographic Textures, Microstructure and Mechanical Properties of Low-Carbon Boron-Bearing Steels

Mandana Zebarjadi Sar *, Silvia Barella, Andrea Gruttadauria, Davide Mombelli and Carlo Mapelli

Department of Mechanical Engineering, Polytechnic University of Milan, 20156 Milan, Italy; silvia.barella@polimi.it (S.B.); andrea.gruttadauria@polimi.it (A.G.); davide.mombelli@polimi.it (D.M.); carlo.mapelli@polimi.it (C.M.)

* Correspondence: mandana.zebarjadi@polimi.it

Received: 1 October 2018; Accepted: 6 November 2018; Published: 9 November 2018

Abstract: The effect of the warm rolling process on the microstructure and the mechanical properties of low-carbon high-boron steels are studied in this work. To investigate these effects, boron-bearing low-carbon steel, subjected to roll at three different temperatures, was studied symmetrically and asymmetrically. The results of the experimental trials achieved by mechanical and microstructural analysis revealed that the use of warm rolling can represent a favorable method to suppress strain aging completely, and to eliminate the fluting effect and yield point elongation. In addition, the tensile and elongation properties are modified with the formation of boron nitride precipitates and dislocations in different thermomechanical conditions.

Keywords: low-carbon steel; warm rolling; boron nitride; dislocation

1. Introduction

The well-known phenomenon of the yield point in low-carbon steels arises from strain aging. The lock of dislocations through the interstitial atoms, i.e., carbon and nitrogen, causes the formation of a Cottrell atmosphere around the dislocation core, leading to a decrease in ductility and the formation of fluting lines in low-carbon steel sheets. According to the Cottrell and Bilby assumption, the kinetics of Cottrell atmosphere formation depends on the number of interstitial atoms moving towards the dislocation core and on the dislocation density [1–4].

The relationship between the strain aging resistance and the chemical composition of steels has been investigated in several studies. The micro alloying elements (Al, Ti, Nb, V), via the formation of carbide and nitride precipitates, cause a decrease in the yield point elongation and an increase in ductility whenever fewer dislocations are pinned by a low amount of interstitial atoms [2,5–7].

Boron has been used as a carbide- and nitride-forming element to reduce strain aging through the extraction of interstitial atoms from solid solutions. Formation of boron nitride provides nucleation sites for Fe_3C and consequently decreases dissolved carbon atoms in solid solution [8–10]. It has been revealed that the addition of boron has an effective influence on decreasing the yield point elongation, which is the result of interstitial atom reduction in a solid solution [11,12]. Moreover, boron has a desirable effect on elongation property when the B/N ratio has the proper value. The reduction of dissolved C,N at grain boundaries and the change of carbide sites from a grain boundary to a ferrite matrix has a major role in the improvement of elongation in boron-bearing steels [10,11,13–15].

In addition to the change in low-carbon steel compositions, experimental work undertaken previously has shown that thermo-mechanical processing can be exploited to modify the mechanical properties of low-carbon steels. Rolling in an intercritical region ($\alpha + \gamma$) is a type of thermomechanical processing in which strengthening is achieved via formation of refined ferrite grains and high dislocation density. However, steels with fine grains exhibit large yield point elongation and low total elongation [16–18]. Fine-grained structures can also be obtained by the use of asymmetric rolling. The additional shear strain has an effective role in improving the strengthening properties with the formation of refined grains and deep-drawability properties with appearance of γ fiber in steels rolled asymmetrically [19–24].

Different methods have been used to eliminate fluting marks in low-carbon steels, such as temper rolling and rolling leveler. These methods eliminate fluting lines through the creation of residual stresses. Temper rolling induces a larger value of residual stresses. Therefore, the fluting defect does not appear for a longer period of time. The small rolls can also induce a large amount of residual stresses and can be effective for the reduction of fluting over a long time. Although these solutions are suggested to eliminate fluting, lines reappear on the steel surface after a while [25].

Considering solutions employed previously, this work focuses on applying a method with the aim of eliminating the fluting defects without using temper rolling. For this purpose, intercritical region rolling of boron-containing steels is substituted by hot rolling, cold rolling, annealing and temper rolling. This work investigates the effect of dislocation density, the effect of the boron nitride size on the mechanical and microstructural properties, and on the crystallographic texture characteristics of the specimens produced by warm rolling symmetrically and asymmetrically. Optimized thermomechanical conditions (rolling temperature, rolling velocity ratio) have been stated to improve the mechanical properties of the rolled samples. To achieve this aim, mechanical, microstructure and texture analyses have been performed.

2. Materials and Methods

The chemical composition of the used low-carbon high-boron steels warm rolled in the lab is presented in Table 1. They were received in the form of (250 × 30 × 2) mm strips.

Table 1. Elemental composition of boron-bearing low-carbon steel (wt. %).

C	Mn	Si	P	S	Cu	Al	Nb	V	Ti	B	N
0.06	0.3	0.03	0.02	0.02	0.04	0.05	0.005	0.005	0.000	0.0035	0.005

To determine the intercritical region ($\alpha + \gamma$) for warm rolling, a Differential Scanning Calorimetry analysis was conducted. This test was done by reheating the samples to 1060 °C at a heating rate of 10 °C/min and cooling at the same rate to room temperature. The achieved curve from DSC test is shown in Figure 1. The intercritical region temperature is considered between the peak of T = 774 °C in cooling process and the peak of T = 926 °C in heating process.

To roll the samples in the intercritical region, the strips were reheated to 1000 °C for 5 min to austenitize them, and they were then kept in the furnace for 2 min at the selected rolling temperatures. The roll of the samples was performed by using two rolling passes symmetrically with equal rolling velocity ratio (1:1) and asymmetrically with a different rolling velocity ratio (1.5:1). In each passage, the specimens were reheated to the desired rolling temperature for 2 min.

To evaluate the fluting intensity, the samples underwent a bending test to determine the fluting value. The specimens were bent around a 50-mm-diameter cylinder, and the contact angle between the sheet and the cylinder was set at 180°. The fluting intensity is measured as the average value (on 15 measurements) of the width of the fluting segments.

The microstructural analysis and the measurement of the ferrite grain size were performed by optical microscope. To observe the steel microstructure, the polished surfaces of the samples were

etched by 2% Nital solution and the measurement of the grain size was performed by the mean linear intercept method (ASTM E112-12).

Tensile specimens with a gauge length of 50 mm and a width of 25 mm were prepared from rolled strips. The tensile test was performed at room temperature at a crosshead displacement rate of 2 mm/min. The test was conducted to determine the tensile strength and elongation of the rolled samples. The Yield Point Elongation (YPE) was assessed from the tensile tests. YPE was measured according to the International UNI EN ISO 6892-1 standard.

The Electron Back-Scattered Diffraction (EBSD) technique was employed for the analysis of the texture of the steel sheets deformed in different thermomechanical conditions. The deformed samples, after polishing by colloidal Silica suspension, were investigated through the use of EBSD operating at an acceleration voltage of 20 Kev and 500× magnification. The dislocation accumulation and boron nitride precipitates were analyzed by transmission electron microscopy (TEM) for different rolling temperatures. Thin foils with the thickness of 100 µm were twinjet electro polished using 10% $HClO_4$ in methanol solution at −20 °C and at 15 V. TEM characterizations were performed with a Philips CM 200 FEG electron microscope using an accelerating voltage of 200 KV.

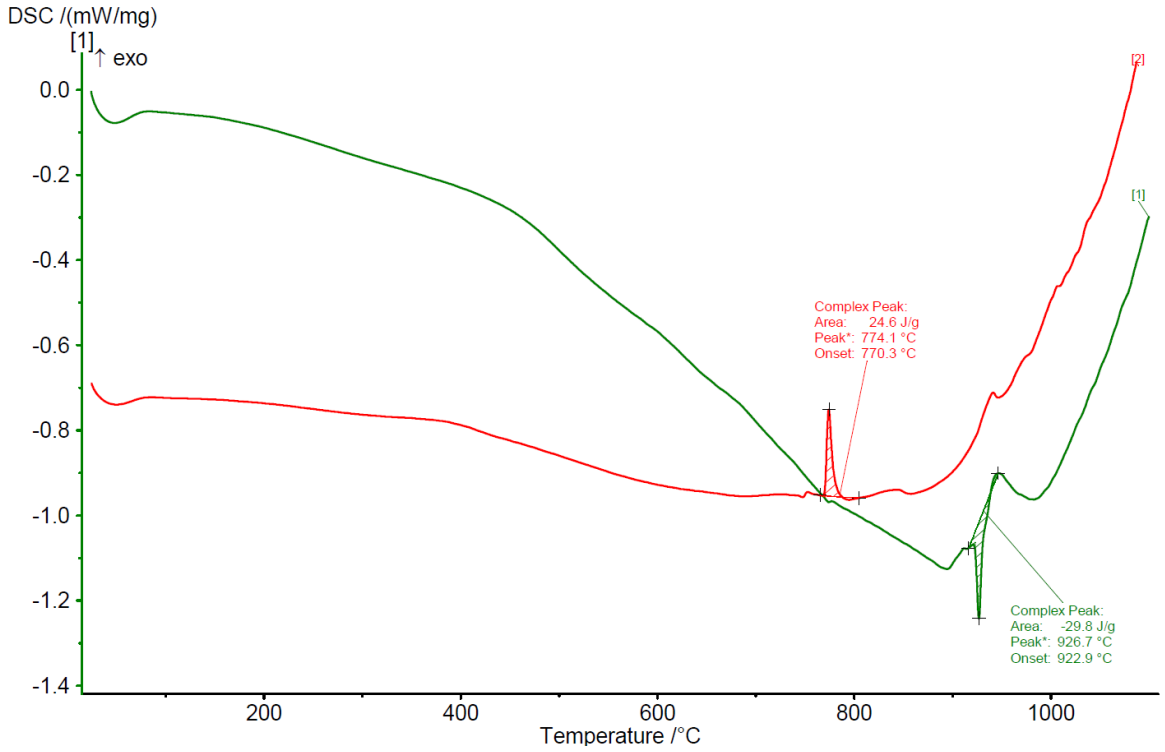

Figure 1. DSC diagram of boron-bearing low-carbon steel.

3. Results

3.1. Microstructure

The optical micrographs of the steels deformed in different thermomechanical conditions are shown in Figure 2. The morphology and the size of the grains change as the function of the rolling temperature and the rolling velocity ratio. The microstructure of the ferrite grains reveal shear bands at lower initial rolling temperatures of 790 °C and 830 °C. These bands are eliminated inside the recrystallized grains formed at a rolling temperature of 870 °C. In addition, the bi-dimensional grains, including the coarse and elongated grains and the fine grains, appear at lower temperatures. When the deformation temperature increases to 870 °C, the homogeneous microstructure of specimens containing fine and equi-axed grains (free of shear bands) is formed by recrystallization. In addition to

the rolling temperature, the rolling rate controls the microstructure of the samples by a variation of the grains size.

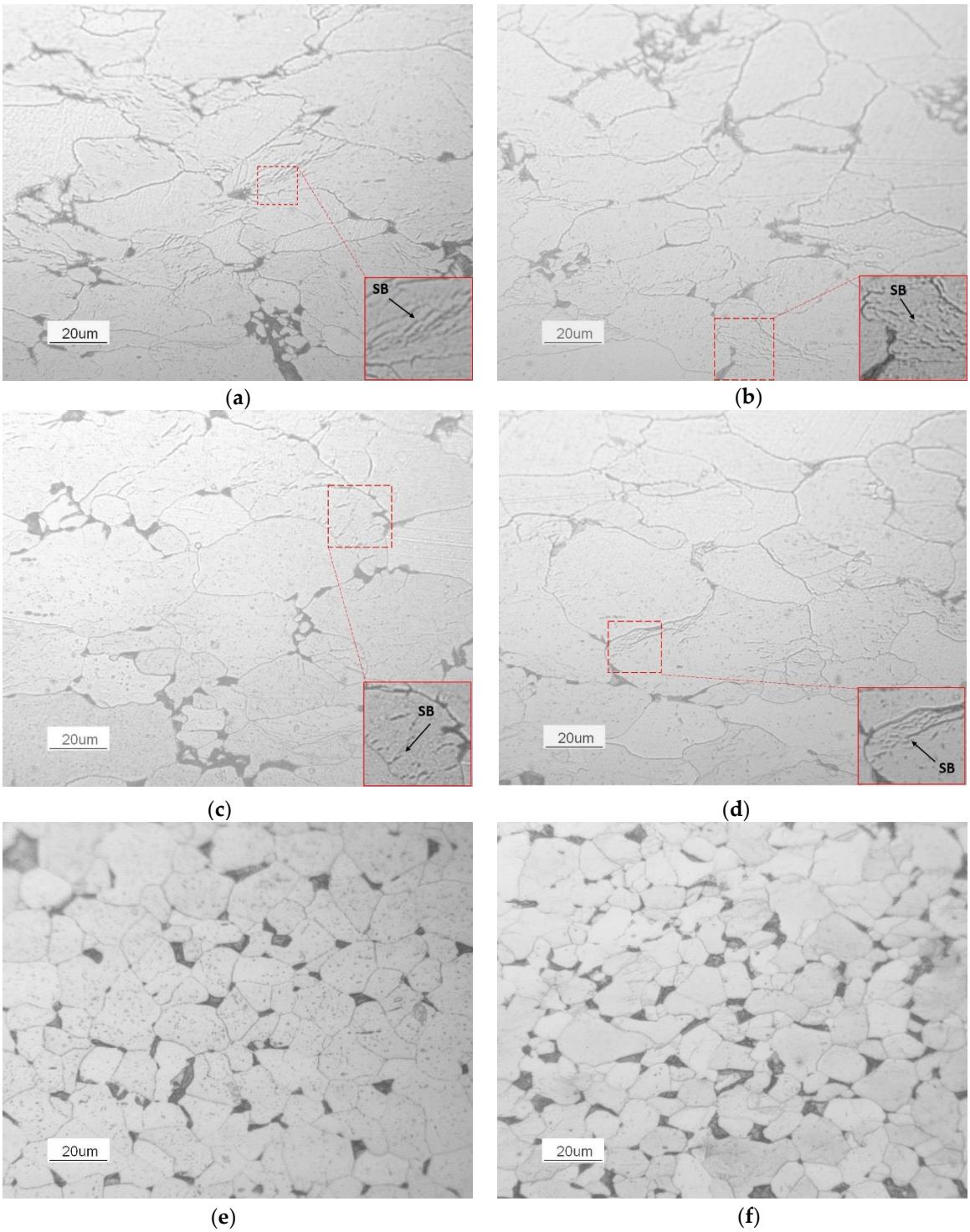

Figure 2. Optical micrographs of LCHB steels warm rolled at (**a**) 790 °C, 1000:1000 rpm, (**b**) 790 °C, 1500:1000 rpm, (**c**) 830 °C, 1000:1000 rpm, (**d**) 830 °C, 1500:1000 rpm, (**e**) 870 °C, 1000:1000 rpm, (**f**) 870 °C, 1500:1000 rpm.

The use of asymmetric rolling with a speed ratio of 1.5 leads to a reduction of grain size under all rolling temperature conditions, as reported in Table 2.

Table 2. Mean equivalent diameter (D_0) of the ferrite grains in terms of rolling temperature and rolling speed ratio.

Rolling Speed Ratio (rpm)	Ferrite Grain Size (μm) (790 °C)	Ferrite Grain Size (μm) (830 °C)	Ferrite Grain Size (μm) (870 °C)
1	31.8 ± 2.3	37.8 ± 3.5	15.9 ± 0.9
1.5	26.7 ± 4.3	31.8 ± 2.9	11.2 ± 0.6

The TEM micrographs exhibit the changes in their microstructures, containing dislocations and boron precipitates at different deformation temperatures. TEM analysis is performed for the symmetrically rolled samples, as the microstructure of the rolled samples with different rolling velocity ratios are the same. Figure 3 shows the dislocation distribution in the grains of the steels deformed at rolling temperatures of 790 °C, 830 °C and 870 °C. The dislocations are accumulated within the grains and close to the grain boundaries. Under all rolling temperature conditions, the entanglement of dislocations leads to the formation of cell structures. As the steel is rolled at a higher rolling temperature, the dislocation density decreases as the cell structure size grows.

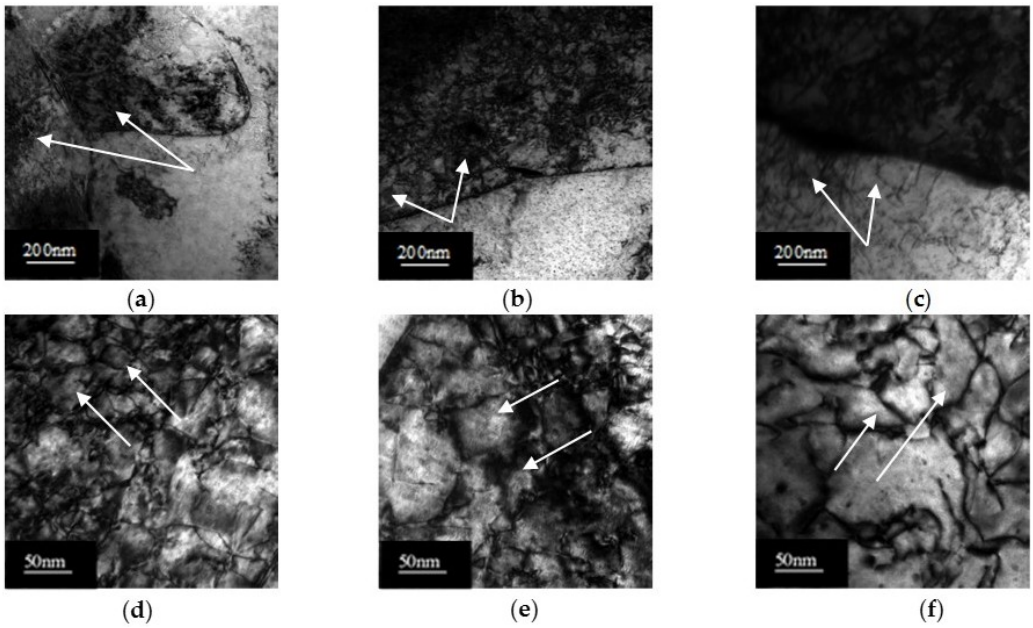

Figure 3. TEM micrographs of LCHB steel showing the dislocation distribution close to the grain boundaries (**a**) rolled at RT = 790 °C, rolling rate ratio = 1000:1000, (**b**) rolled at RT = 830 °C, (**c**) rolled at RT = 870 °C; and cell structure of dislocations (**d**) rolled at RT = 790 °C, rolling ratio = 1000:1000, (**e**) rolled at RT = 830 °C, rolling ratio = 1000:1000, (**f**) rolled at RT = 870 °C, rolling ratio = 1000:1000. The cell structures in all images are indicated by the arrows.

In Figure 4, the dislocation network distribution with fine precipitates at different rolling temperatures is seen. Fine precipitates disperse on the grain boundary and on the dislocation networks close to the grain boundaries at lower rolling temperatures. By contrast, the grain boundary and the cell walls located near the grain boundary are free of fine precipitates in the steel deformed at a rolling temperature of 870 °C.

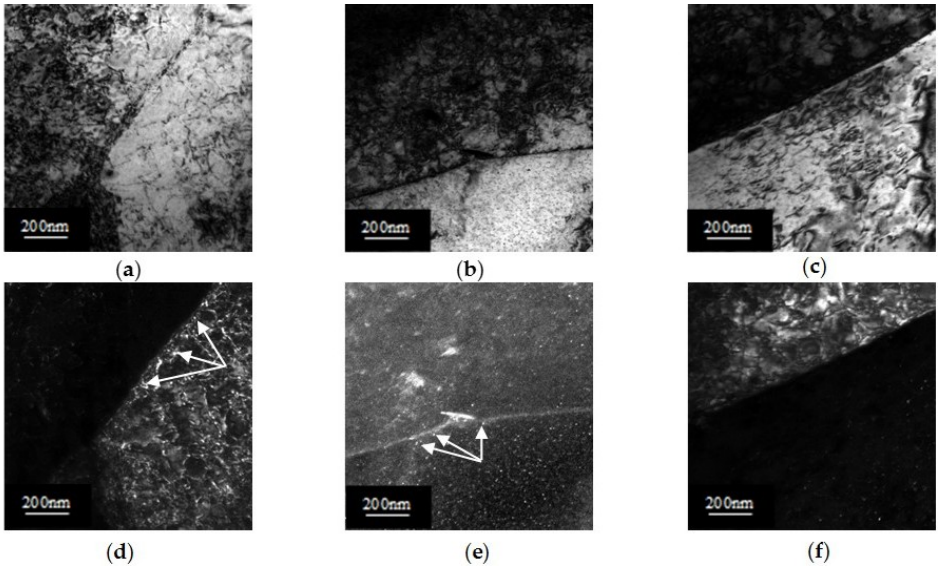

Figure 4. TEM micrographs of LCHB steel showing the dislocation network distribution with precipitates close to the grain boundaries, (**a**) bright field image of steel rolled at RT = 790 °C, (**b**) bright field image of steel rolled at RT = 830 °C, (**c**) bright field image of steel rolled at RT = 870 °C, (**d**) dark field image of steel rolled at RT = 790 °C, (**e**) dark field image of steel rolled at RT = 830 °C, (**f**) dark field image of steel rolled at RT = 870 °C. The precipitates are indicated by arrows.

The precipitate distribution within and on the dislocations of the cell walls with their selected area electron diffraction patterns can be observed in Figure 5. The index of the obtained diffraction patterns shows that the observed precipitates in all the samples are boron nitride (BN), with a tetragonal structure and a lattice parameter of a_0 = 2.57 Å. The precipitates attributed to the steel deformed at the highest temperature are revealed to be the coarse particles on the dislocations. By contrast, the fine precipitates are dispersed on and between the dislocations in the steels deformed at lower temperatures.

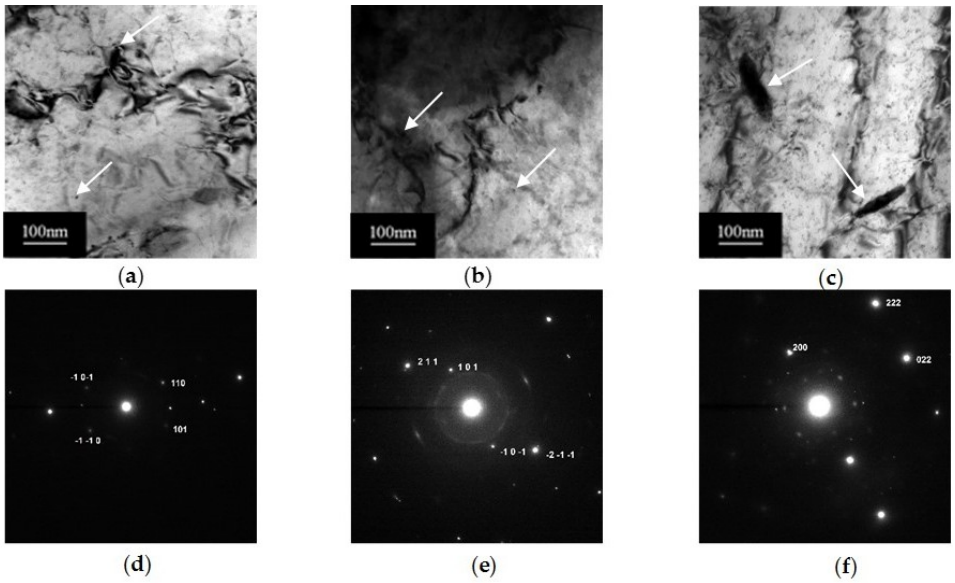

Figure 5. TEM micrographs of LCHB steel exhibiting distribution of dislocations and BN precipitates: (**a**) bright field image of steel rolled at RT = 790 °C, (**b**) bright field image of steel rolled at RT = 830 °C, (**c**) bright field image of steel rolled at RT = 870 °C, (**d**) the correlated SAED of steel rolled at RT = 790 °C (zone axis = [1^{-}11]), (**e**) the correlated SAED of steel rolled at RT = 830 °C (zone axis = [$^{-}$1^{-}11]), (**f**) the correlated SAED of steel rolled at RT = 870 °C (zone axis = [011]).

3.2. Texture

Figure 6 presents the texture components of the samples undergoing different thermomechanical conditions in orientation distribution function sections of ϕ_2 = 45°. The conventional rolling that induces the compression stress develops the texture components including {112} <131>, {111} <112>, {111} <110> and {112} <110> at a temperature of 830 °C. The intensity of {112} <131> and {111} <112> components is reduced when the plastic deformation is employed above the recrystallization temperature of 870 °C. In addition to the represented components, the component of {001} <110> is formed as the recrystallized component of {100} <001>.

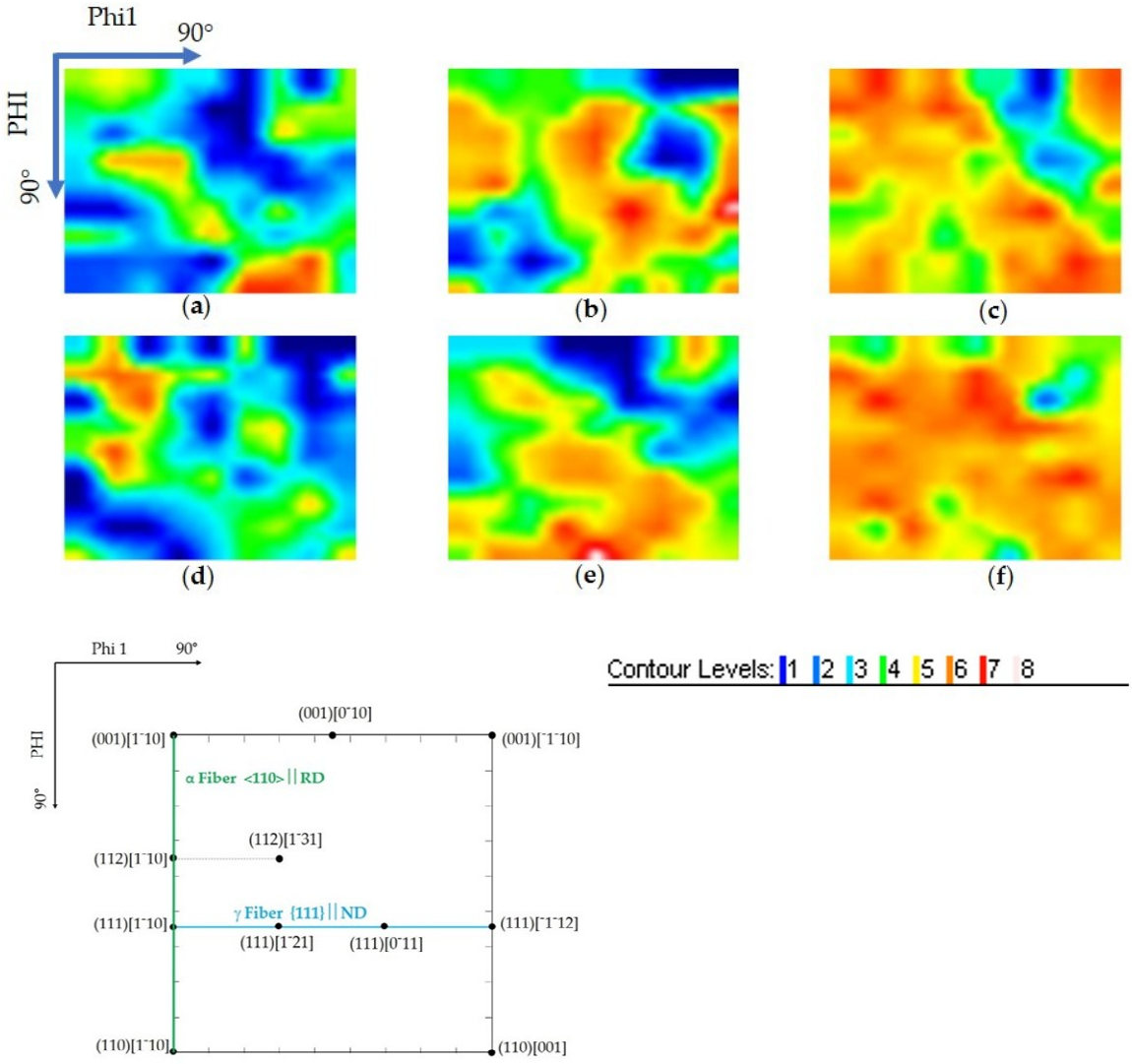

Figure 6. Texture components and fiber characteristics of a rolled plate in the orientation distribution function (ODF) sections of the Euler space of Phi2 = 45° at (**a**) 790 °C, 1000:1000 rpm, (**b**) 830 °C, 1000:1000 rpm, (**c**) 870 °C, 1000:1000 rpm, (**d**) 790 °C, 1500:1000 rpm, (**e**) 830 °C, 1500:1000 rpm, (**f**) 870 °C, 1500:1000 rpm according to the bcc production orientations in ϕ_2 = 45° [26,27].

With the use of differential speed rolling, the rotated cube component also appears in non-recrystallized temperatures. The intensity of the {112} <131> component reduces in comparison with equal speed rolling conditions and the components of {111} <112> and {112} <110> are eliminated. As the rolling temperature increases to 870 °C, in addition to the former texture components formed at a conventional rolling condition, γ fiber appears.

The percentage of grain boundary misorientation angles (θ) in samples formed by different rolling temperatures and different rolling velocity ratios is shown in Figure 7. The percentage of low-angle grain boundaries with θ < 15° is greater in the samples deformed at lower rolling temperatures and symmetric rolling. Conversely, the percentage of high-angle grain boundaries with 15° < θ < 60° is revealed to be greater in the microstructure of the samples containing fragmented grains formed with asymmetric rolling and in the samples composed of recrystallized grains formed at the highest rolling temperature.

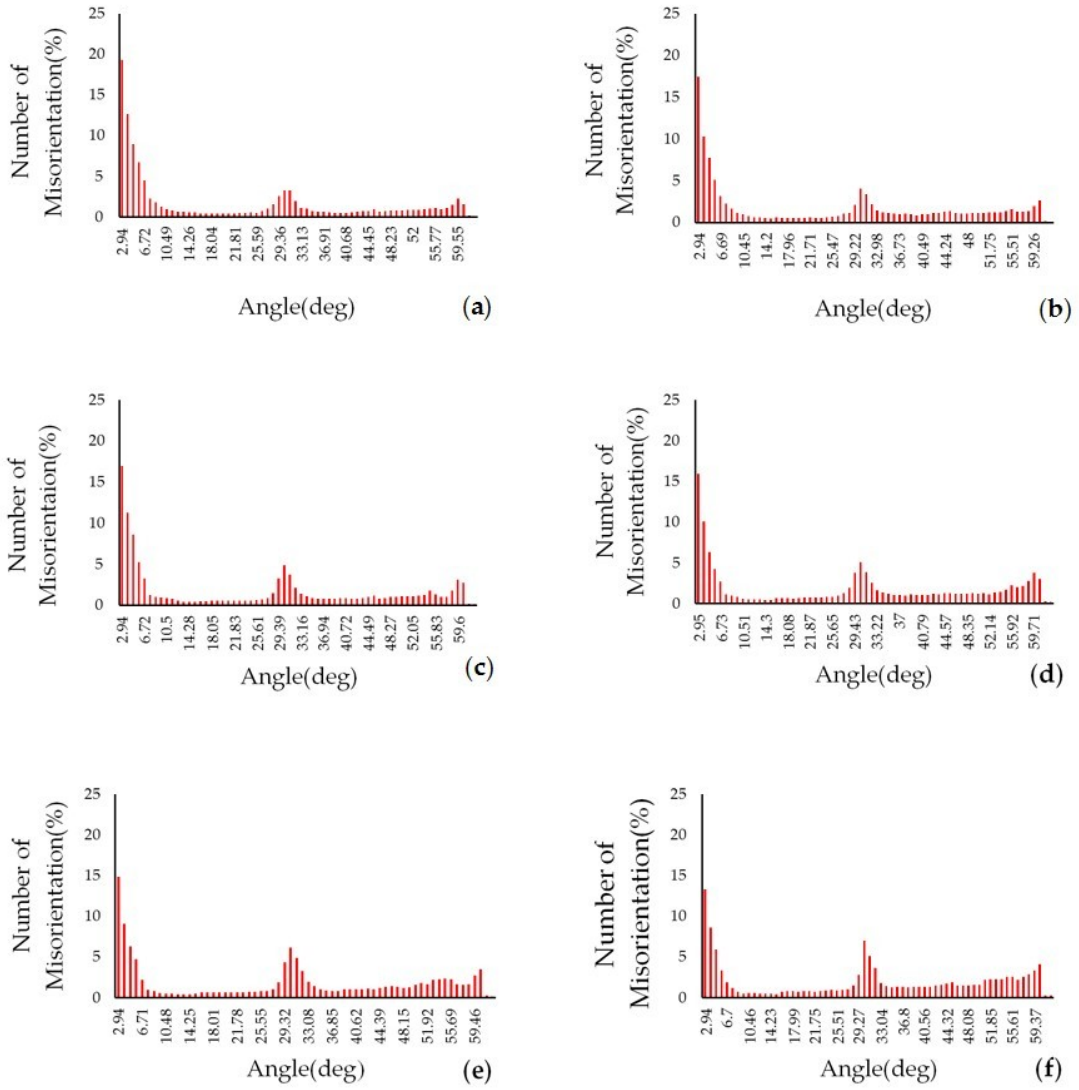

Figure 7. Misorientation distribution of steel strips deformed at (**a**) RT = 790 °C, symmetric rolling, (**b**) RT = 790 °C, asymmetric rolling, (**c**) RT = 830 °C, symmetric rolling, (**d**) RT = 830 °C, asymmetric rolling, (**e**) RT = 870 °C, symmetric rolling, (**f**) RT = 870 °C, Asymmetric rolling.

3.3. Tensile Properties

The tensile properties of the samples are affected by the thermomechanical parameters applied in this work. Figure 8a shows the yield strength in terms of rolling temperature for the steel sheets rolled with two different rolling speed ratios. With an increase in the initial rolling temperature from 790 °C to 870 °C, the yield strength decreases from 484 MPa to 379 MPa in symmetrically rolled samples and decreases from 587 MPa to 437 MPa in the samples rolled asymmetrically.

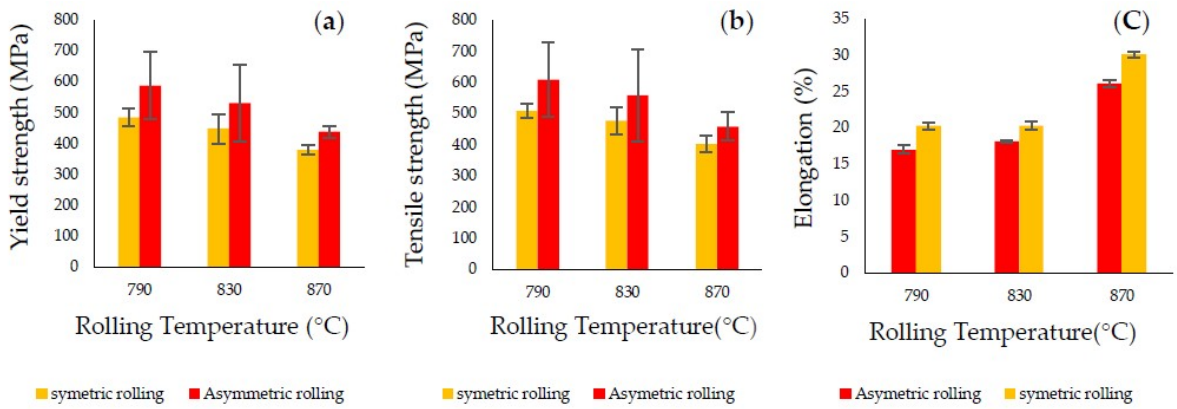

Figure 8. The effect of rolling temperature and rolling speed ratio on (**a**) yield strength values, (**b**) tensile strength values, (**c**) elongation values of warm rolled steels.

The value of the employed rolling velocity affects the yield strength of the samples as well. The sheets subjected to equal-speed rolling have a lower yield strength compared to the steels deformed by differential-speed rolling. As depicted in Figure 8b, the tensile strength has the same behavior in terms of deformation temperature. It declines with the increase of the rolling temperature. The ultimate tensile strength is also affected by the amount of induced stress. It is increased by employing asymmetric rolling, according to the Hall-Petch relation.

The total elongation increases when the rolling temperature increases from 790 °C to 870 °C. This property is also affected by the rolling speed ratio. A decrease in elongation happens when asymmetric rolling is employed.

The rolling temperature and the rolling velocity ratio likewise have an impact on the yield point elongation % and fluting intensity. The yield point elongation is eliminated in all the samples subjected to different thermomechanical conditions. The continuous yielding phenomenon (YPE~0) is demonstrated in Figure 9 by a representative diagram of the sample rolled asymmetrically at rolling temperature of 790 °C.

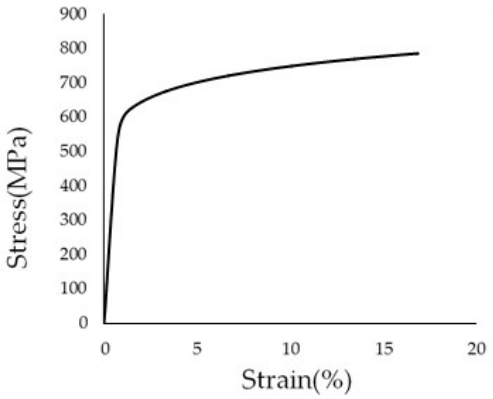

Figure 9. Continuous yielding behavior of low-carbon boron-bearing steel deformed asymmetrically at a rolling temperature of 790 °C.

The fluting intensity of boron-containing steel sheets is also affected by the thermomechanical parameters. The surface of all the steels demonstrated in Figure 10 are flat and free from fluting lines (fluting intensity ~0).

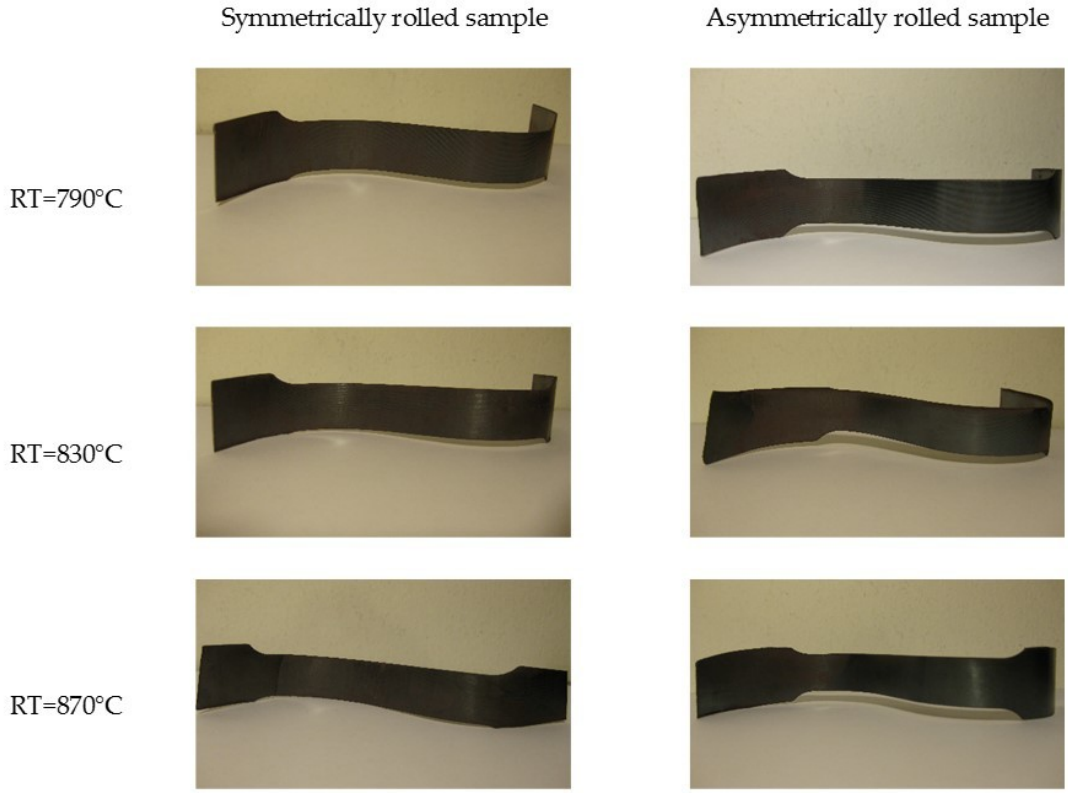

Figure 10. The flat surfaces of the strips bent under different thermomechanical conditions with no fluting segments in the high-boron low-carbon steel.

4. Discussion

4.1. Microstructure and Crystallographic Texture

The grains containing the shear bands have a higher dislocation density. The intersection of these bands divides the interior of the grains from the cell substructures with accumulation of dislocations in the cell blocks [28]. An increase in the rolling temperature increases the climb and cross glide of dislocations, which leads to a reduction in the shear bands and to cell substructure growth [29,30]. In addition, the greater entanglement of dislocations in the steel deformed at lower temperatures might be due to the presence of the fine precipitates, which play a major role in the pinning of dislocations and the wall of cell structures. The fine precipitates also have different deformability compared to the ferrite matrix, and they pile up dislocations near their locations [15,28].

The insertion of dislocations, rearranged as cellular structures, increases the stored energy of the microstructure and provides the nucleation sites for the formation of the fine grains near the grain boundaries [31]. However, the growth of the fine grains is impeded by the fine precipitates acting as the pinning points on their grain boundaries [32]. In contrast, the formation and the growth of the new grains due to the recrystallization phenomenon happen at a rolling temperature of 870 °C. This indicates the mobility of the dislocations and the cell walls bounded by the coarse precipitates. The coarse boron nitride precipitates do not strongly interact with the dislocations. Therefore, the recrystallization phenomenon is not impeded by these particles. Moreover, no precipitates are found along the grain boundary at this rolling temperature; hence, the mobility and the bulge of the grain boundaries for the formation of the recrystallized grains occur [33,34]. The measurements performed on the size of the grains show that asymmetric rolling reduces the grains size. The simple shear subjected to asymmetric rolling induces the local rotation of the grain fragments. The rotation of adjacent grain fragments intensifies the lattice curvature of their boundaries and forms fine grains [35].

The ODF maps of the samples rolled asymmetrically reveal the {001} <110> component at all rolling temperatures. The accumulation of strain due to the use of asymmetric rolling favors the formation of this recrystallized texture [26]. During asymmetric rolling above the recrystallized temperature, the reinforcement of γ fiber with a high value of r_m and a low value of Δr improves the property of drawability; consequently, plate rolled under these thermomechanical conditions could be desirable for applications in which high formability is required [26].

As observed in Figure 7, the grains deformed at low rolling temperatures possess a large amount of low grain boundaries. This effect depicts the sub-grain boundaries formed by the cell substructures within the grains, and in addition, the main grain boundaries cannot be oriented compared to other grains, as they are pinned by the fine boron nitride precipitates. However, by increasing the temperature to recrystallization temperature, the number of HAGBs increases, thanks to the formation of coarse boron nitride precipitates and to the annihilation of the pinning effect, resulting in grain boundary migration and the formation of new grains with different orientations when compared to the neighboring grains. The misorientation of the grain boundaries also increases when the strip is deformed by asymmetric rolling. Asymmetric rolling through the simple shear deformation mode creates a higher percentage of high-angle grain boundaries. This effect could be due to the fact that asymmetric rolling produces a non-symmetric velocity gradient component (rotation rate). As the material is subjected to simple shear deformation, the velocity gradient occurs in the medium layer of the material because of the presence of different shear deformation behavior. On the contrary, the pure shear induced by symmetric rolling provides the symmetric component of the velocity gradient (strain rate). In this case, the rotation of grains is restrained [35–38].

4.2. Tensile Properties

The strengthening mechanism is attributed to precipitation strengthening, dislocation strengthening, solid-solution strengthening, and the stress connected to the grain size. In this case, two mechanisms of precipitation strengthening and dislocation strengthening contribute to improve the tensile properties of the samples at lower temperatures. As observed in TEM micrographs of samples rolled at lower temperatures, the fine precipitates of boron nitride are dispersed on the dislocations within the grains. These fine precipitates pin the dislocation to move, so they strengthen the samples, but by coarsening the precipitate size at a rolling temperature of 870 °C, the strengthening effect decreases, which is in agreement with the Orowan-Ashby equation [39]. In addition to the fine precipitates, the high dislocation densities in specimens deformed at rolling temperatures of 790 °C and 830 °C increase the strength properties.

At the highest rolling temperature, the strength decreases, thanks to the formation of a lower density of dislocations. Therefore, there is less interaction between dislocations. This phenomenon is explained by the Taylor equation [40].

The total elongation results show that the accumulation of dislocations caused by an intensive interaction among the dislocations and the precipitations reduces the dislocation movement. This effect results in lower total elongation in the steels deformed at lower rolling temperatures.

The elimination of YPE% and fluting marks is attributed to the B:N ratio and thermomechanical conditions employed in this work. In the work done by Chown and Cornish, boron completely removed free nitrogen atoms with the formation of boron nitride precipitates when the stoichiometric ratio between B:N was more than 0.75 [41]. Since the B:N ratio for the selected samples is 0.7, the use of warm rolling in different thermomechanical conditions (rolling temperature, rolling velocity ratio) removes the impact of the remaining free nitrogen to form the Cottrell atmosphere effect. The elimination of the yield point elongation can be attributed to the formation of mobile dislocations, produced through the warm rolling, that are not pinned by the remaining nitrogen atoms. In addition, the presence of fluting marks depends on the mobile dislocations that are not pinned by the interstitial atoms. As the amount of free nitrogen atoms is more than the value that could be eliminated completely by the addition of boron, these steels are prone to revealing fluting lines, but the remaining free nitrogen

atoms do not make the surface rough. This effect is due to the induction of mobile dislocations that are multiplied by the rolling process, and the amount of free nitrogen is not enough to pin the mobile dislocations.

5. Conclusions

In this study, the effect of the boron nitride precipitates and of the dislocation densities on the mechanical properties of the low-carbon high-boron steel has been investigated. The achieved results are summarized as follows:

(1) The fine boron nitride precipitates, by their pinning effect, improve the strength properties of the steel deformed at lower rolling temperatures.
(2) High dislocation densities, forming smaller cell structures in specimens deformed at rolling temperatures of 790 °C and 830 °C, enhance the strength properties.
(3) The use of boron-added steel is beneficial when the stoichiometric ratio of boron with nitrogen is equal to 0.7. This condition provides the best opportunity for the complete elimination of the fluting effect and the yield point elongation when warm rolling is applied.
(4) Asymmetric rolling through the creation of the simple shear only affects the size of the grains via formation of refined grains at all rolling temperatures.
(5) The deformation modes influence the boundary characters. The simple shear due to the creation of the velocity gradient causes the formation of larger numbers of high angle grain boundaries.
(6) Asymmetric and symmetric rolling have the same effect on the trend of mechanical properties at all rolling temperatures.

Author Contributions: Methodology, formal analysis, investigation, data curation, writing—original draft preparation, project administration, M.Z.S.; resources, A.G.; writing—review and editing, D.M.; supervision, C.M. and S.B.

Funding: This research received no external funding.

Acknowledgments: The steel sheets used in this project were supplied by Ilva factory.

Conflicts of Interest: The authors declare no conflict of interest.

References

1. Zhao, J.Z.; De, A.K.; De Cooman, B.C. Formation of the Cottrell Atmosphere during Strain Aging of Bake-Hardenable Steels. *Metall. Mater. Trans. A* **2001**, *32*, 417–423. [CrossRef]
2. Baker, L.J.; Daniel, S.R.; Parker, J.D. Metallurgy and Processing of Ultralow Carbon Bake Hardening Steels. *Mater. Sci. Technol.* **2002**, *18*, 355–368. [CrossRef]
3. Zhao, J.Z.; De, A.K.; Cooman, B.D. A Model for the Cottrell Atmosphere Formation during Aging of Ultra Low Carbon Bake Hardening Steels. *ISIJ Int.* **2000**, *40*, 725–730. [CrossRef]
4. Baker, L.J.; Parker, J.D.; Daniel, S.R. Mechanism of Bake Hardening in Ultralow Carbon Steel Containing Niobium and Titanium Additions. *Mater. Sci. Technol.* **2002**, *18*, 541–547. [CrossRef]
5. Gündüz, S.; Cochrane, R.C. Effect of Dynamic Strain Aging on Mechanical Properties of Vanadium Microalloyed Steel. *Mater. Sci. Technol.* **2003**, *19*, 422–428. [CrossRef]
6. Karabulut, H.; Gündüz, S. Effect of vanadium content on dynamic strain ageing in microalloyed medium carbon steel. *Mater. Des.* **2004**, *25*, 521–527. [CrossRef]
7. Gündüz, S. Dynamic Strain Aging Effects in Niobium Microalloyed Steel. *Ironmak. Steelmak.* **2002**, *29*, 341–346. [CrossRef]
8. Haq, M.I.; Ikram, N. The Effect of Boron Addition on the Tensile Properties of Control-Rolled and Normalized C-Mn Steels. *J. Mater. Sci.* **1993**, *28*, 5981–5985. [CrossRef]
9. de Souza, T.O.; Buono, V.T.L. Optimization of the Strain Aging Resistance in Aluminum Killed Steels Produced by Continuous Annealing. *Mater. Sci. Eng. A* **2003**, *354*, 212–216. [CrossRef]
10. Funakawa, Y.; Inazumi, T.; Hosoya, Y. Effect of Morphological Change of Carbide on Elongation of Boron-Bearing Al-Killed Steel Sheets. *ISIJ Int.* **2001**, *41*, 900–907. [CrossRef]

11. Pitakkorraras, S.; Hirunlabh, C.; Umeda, T. Microstructure observation and mechanical properties of hot rolled low carbon steel strip with boron addition. Proceedings of METAL 2011, Brno, Czech Republic, 18–20 May 2011.
12. Nuntawat, C.; Umeda, T. Development in Production of High Formability Boron Added Low Carbon Steel. Proceedings of METAL 2013, Brno, Czech Republic, 15–17 May 2013.
13. Deva, A.; De, S.K.; Jha, B.K. Effect of B/N Ratio on Plastic Anisotropy Behaviour in Low Carbon Aluminium Killed Steel. *Mater. Sci. Technol.* **2008**, *24*, 124–126. [CrossRef]
14. Deva, A.; De, S.K.; Jha, B.K. Strain Hardening Behavior and Cold Reducibility of Boron-Added Low-Carbon Steel. *J. Mater. Eng. Perform.* **2009**, *18*, 109–110. [CrossRef]
15. Deva, A.; Jha, B.K.; Mishra, N.S. Influence of Boron on Strain Hardening Behaviour and Ductility of Low Carbon Hot Rolled Steel. *Mater. Sci. Eng. A* **2011**, *528*, 7375–7380. [CrossRef]
16. Bakkaloğlu, A. Effect of Processing Parameters on the Microstructure and Properties of an Nb Microalloyed Steel. *Mater. Lett.* **2002**, *56*, 200–209. [CrossRef]
17. Song, R.; Ponge, D.; Raabe, D.; Speer, J.G.; Matlock, D.K. Overview of Processing, Microstructure and Mechanical Properties of Ultrafine Grained Bcc Steels. *Mater. Sci. Eng. A* **2006**, *441*, 1–17. [CrossRef]
18. Panigrahi, B.K. Processing of Low Carbon Steel Plate and Hot Strip—An Overview. *Bull. Mater. Sci.* **2001**, *24*, 361–371. [CrossRef]
19. Hamad, K.; Ko, Y.G. Effect of Roll Speed Ratio on Microstructure Evolution and Mechanical Properties of 0.18 wt% Carbon Steel Deformed by Differential Speed Rolling. *Mater. Lett.* **2015**, *160*, 213–217. [CrossRef]
20. Ding, Y.; Jiang, J.; Shan, A. Microstructures and Mechanical Properties of Commercial Purity Iron Processed by Asymmetric Rolling. *Mater. Sci. Eng. A* **2009**, *509*, 76–80. [CrossRef]
21. Cai, M.H.; Dhinwal, S.S.; Han, Q.H.; Chao, Q.; Hodgson, P.D. Gradient Ultrafine Ferrite and Martensite Structure and Its Tensile Properties by Asymmetric Rolling in Low Carbon Microalloyed Steel. *Mater. Sci. Eng. A* **2013**, *583*, 205–209. [CrossRef]
22. Chen, S.; An, Y.G.; Lahaije, C. Toughness Improvement in Hot Rolled HSLA Steel Plates through Asymmetric Rolling. *Mater. Sci. Eng. A* **2015**, *625*, 374–379. [CrossRef]
23. Lee, K.-M.; Lee, H.-C. Grain Refinement and Mechanical Properties of Asymmetrically Rolled Low Carbon Steel. *J. Mater. Process. Technol.* **2010**, *210*, 1574–1579. [CrossRef]
24. Orlov, D.; Pougis, A.; Lapovok, R.; Toth, L.S.; Timokhina, I.B.; Hodgson, P.D.; Haldar, A.; Bhattacharjee, D. Asymmetric Rolling of Interstitial-Free Steel Using Differential Roll Diameters. Part I: Mechanical Properties and Deformation Textures. *Metall. Mater. Trans. A* **2013**, *44*, 4346–4359. [CrossRef]
25. Hundy, B.B. Elimination of stretcher strains in mild-steel pressings. *J. Iron Steel Inst.* **1954**, *178*, 127–138.
26. Jj, J.; Mp, B.-G.; Savoie, J. Transformation Textures in Steels. *ISIJ Int.* **1994**, *34*, 927–942.
27. Randle, V.; Engler, O. *Introduction to Texture Analysis: Macrotexture, Microtexture and Orientation Mapping*; CRC Press: London, UK, 2014.
28. Sakai, T.; Belyakov, A.; Kaibyshev, R.; Miura, H.; Jonas, J.J. Dynamic and Post-Dynamic Recrystallization under Hot, Cold and Severe Plastic Deformation Conditions. *Prog. Mater. Sci.* **2014**, *60*, 130–207. [CrossRef]
29. Zhang, C.; Liu, Z.; Wang, G. Effects of Hot Rolled Shear Bands on Formability and Surface Ridging of an Ultra Purified 21% Cr Ferritic Stainless Steel. *J. Mater. Process. Technol.* **2011**, *211*, 1051–1059. [CrossRef]
30. McQueen, H.J. The Production and Utility of Recovered Dislocation Substructures. *Metall. Trans. A* **1977**, *8*, 807–824. [CrossRef]
31. Bengochea, R.; Lopez, B.; Gutierrez, I. Microstructural Evolution during the Austenite-to-Ferrite Transformation from Deformed Austenite. *Metall. Mater. Trans. A* **1998**, *29*, 417–426. [CrossRef]
32. Pa, M.; Ferry, M.; Chandra, T. Five Decades of the Zener Equation. *ISIJ Int.* **1998**, *38*, 913–924.
33. El-Kashif, E.; Asakura, K.; Koseki, T.; Shibata, K. Effects of Boron, Niobium and Titanium on Grain Growth in Ultra High Purity 18% Cr Ferritic Stainless Steel. *ISIJ Int.* **2004**, *44*, 1568–1575. [CrossRef]
34. Samet-Meziou, A.; Etter, A.L.; Baudin, T.; Penelle, R. TEM Study of Recovery and Recrystallization Mechanisms after 40% Cold Rolling in an IF-Ti Steel. *Scr. Mater.* **2005**, *53*, 1001–1006. [CrossRef]
35. Segal, V. Review: Modes and processes of severe plastic deformation (SPD). *Materials* **2018**, *11*, 1175. [CrossRef] [PubMed]
36. Estrin, Y.; Vinogradov, A. Extreme grain refinement by severe plastic deformation: A wealth of challenging science. *Acta Mater.* **2013**, *61*, 782–817. [CrossRef]

37. Beygelzimer, Y. Vortices and mixing in metals during severe plastic deformation. *Mater. Sci. Forum* **2011**, *683*, 213–224. [CrossRef]
38. Kulagin, R.; Beygelzimer, Y.; Ivanisenko, Yu.; Mazilkin, A.; Straumal, B.; Hahn, H. Instabilities of interfaces between dissimilar metals induced by high pressure torsion. *Mater. Lett.* **2018**, *222*, 172–175. [CrossRef]
39. Gladman, T. Precipitation Hardening in Metals. *J. Mater. Sci. Technol.* **1999**, *15*, 30–36. [CrossRef]
40. Gao, H.; Huang, Y. Taylor-Based Nonlocal Theory of Plasticity. *Int. J. Solids Struct.* **2001**, *38*, 2615–2637. [CrossRef]
41. Chown, L.H.; Cornish, L.A. Investigation of Hot Ductility in Al-Killed Boron Steels. *Mater. Sci. Eng. A* **2008**, *494*, 263–275. [CrossRef]